Microstructural Exploration of the High Capacitance in RuO_2-ZrO_2 Coating①

MA Ji-Dong[a②] WU Yun-Miao[b] JIANG Chun-Hai[a]
ZHANG Hou-An[a] ZHU Jun-Qiu[b②]

[a] (*Fujian Key Laboratory of Functional Materials and Applications, Xiamen University of Technology, Xiamen* 361024, *China*)

[b] (*School of Chemical Engineering and Materials Science, Quanzhou Normal University, Quanzhou* 362000, *China*)

ABSTRACT A high capacitance RuO_2-ZrO_2 coating was prepared by thermal decomposition method. Extended X-ray absorption fine structure (EXAFS), X-ray diffraction (XRD), high-resolution transmission electron microscope (HRTEM) and *ab initio* calculations were applied to understand the role of the microstructure in the acquisition of high specific capacitance of RuO_2-based oxides. The results show that the RuO_2-ZrO_2 oxide prepared at critical crystallization temperature can be considered to be quasi-amorphous or microcrystalline (A short-range ordered crystal structure can be seen from the TEM image, but no diffraction peaks can be seen from the XRD diffraction patterns). And this RuO_2-ZrO_2 was identified as a solid solution with high solid solubility. It referred to herein as a quasi-amorphous solid solution. Such a special microstructure was conducive for "synergistic catalysis" owing to the cationic interaction and thus could gain high "active site density" and high "active surface", thus developing high specific capacitance.

Keywords: supercapacitor, quasi-amorphous, RuO_2, ZrO_2, synergistic catalysis;
DOI: 10.14102/j.cnki.0254–5861.2011–2781

1 INTRODUCTION

With metallic conductivity, excellent electrochemical stability and high theoretical specific capacitance, RuO_2 is recognized as one ideal electrode material for supercapacitor. However, due to agglomeration and low specific surface area, the expected high capacitance is difficult to be achieved on pure RuO_2[1, 2]. Instead, combining RuO_2 with other non-noble metal oxides has been proven to be an effective way to acquire high specific capacitance[3-6]. The added non-noble metal oxides can not only serve as the carrier to increase the dispersibility and electrochemical stability of RuO_2, but can also generate "synergistic catalysis" effect to improve the electronic structure of RuO_2[7, 8]. Both effects are beneficial to activate the oxidization activity, and hence significantly increase the capacitance of RuO_2. So far, TiO_2, SnO_2, Co_3O_4, Ta_2O_5, MnO_2 and SiO_2 have been used as the effective second components[9-12], although their exact roles on the improved capacitance are still in controversy.

In our previous work, the RuO_2-ZrO_2 coating on Ti substrate was prepared by thermal decomposition method and an ultrahigh capacitance of 949 $F \cdot g^{-1}$ was obtained at a critical temperature of about 290 ℃[13, 14]. This high capacitance has been ascribed to the special amorphous structure of the RuO_2-ZrO_2 coating in combination with short range order microcrystallines. However, a detailed microstructural interpre-tation was still lack. In general, the synergistic effect between the amorphous RuO_2 and the second component may play a key role in the high specific capacitance[10, 12]. The amorphous structure can be normally divided into topology and microcrystal according to the degree of order. It can also be divided into amorphous, quasi-amorphous and pseudo-amorphous structure according to the order characteristics. Some researchers also divided it to be XRD amorphous and

Received 24 February 2020; accepted 20 April 2020

① Supported by the National Natural Science Foundation Program of China (51604239) and Program for New Century Excellent Talents in Fujian Province University (NCETFJ) and Program for Innovative Research Team in Science and Technology in Fujian Province University (IRTSTFJ)

② Corresponding authors. Ma Ji-Dong. E-mail: majidong@xmut.edu.cn; Zhu Jun-Qiu, E-mail: junqiu@qztc.edu.cn

TEM amorphous from the perspective of observation. Furthermore, it can be divided into metal glass, inorganic glass and organic glass based on the composition. There are still tremendous mysteries in amorphous structure[15, 16]. Particularly, no convincing conclusion on multiple oxide materials has been achieved yet. Some studies demonstrated that amorphous structure was advantageous in performance mostly because of its structural flexibility[17]. Some others argued that such performance advantage of amorphous structure was contributed by high-concentration lattice defects or large surface area[18]. However, none of these studies discussed the key factor of amorphous structure and the degree of order[19].

To comprehensively understand the effect of amorphous structure of composite oxide, amorphous oxides were analyzed by XRD, HRTEM and EXAFS methods. Traditional structural analysis of the material is mainly based on diffraction phenomenon of long-range order structure and thus it is inapplicable to amorphous structure. By contrast, EXAFS is applicable to both crystal and amorphous structures and is therefore an effective method to explore the local atomic structural information[20]. In addition, as reported, no evident solid solution was generated in the RuO_2-ZrO_2 system[21]. Nevertheless, in our previous thermodynamic study, it was found that the system may gain unstable RuO_2-ZrO_2 with high solid solubility[13]. In other words, thermal decomposition at the critical temperature may retain disordered ions of precursor in composite oxides, resulting in high mutual solubility in the RuO_2-ZrO_2 system. However, such a non-equilibrium phase has not been reported yet. In this paper, the microstructure of non-equilibrium phase was predicted by *ab initio* calculation based on density functional theory (DFT). The microstructure of RuO_2-ZrO_2 coating that has high specific capacitance was analyzed jointly by XRD, HRTEM and EXAFS, as compared to the DFT prediction. The relationship between the performance and the microstructure of the prepared material will be discussed.

2 EXPERIMENTAL

2. 1 Preparation of the electrode materials

The RuO_2-ZrO_2 coating was prepared by thermal decomposition method at a critical temperature of about 290 ℃[13, 14]. In typical, ruthenium trichloride and $ZrCl_4$ with a nominal molar ratio of 5:5 were separately dissolved in absolute ethyl alcohol under ultrasonic vibration. These two solutions were then mixed evenly and held statically at room temperature for 12 h. For comparison, Ti/RuO_2, Ti/ZrO_2 and Ti/RuO_2-ZrO_2 coating electrodes were also prepared at the crystallization temperature of 450 ℃[13, 14]. Due to volatilization of the precursor during thermal decomposition, the Ru/Zr atomic ratio in the amorphous RuO_2-ZrO_2 system was quantitatively analyzed by inductively coupled plasma (ICP) measurement by ARCOS SOP (Germany). The electrochemical property of the composite coatings was studied in 0.5 M H_2SO_4 aqueous solution with a CHI660D electrochemical workstation in a conventional three-electrode system equipped with a Pt foil of 2 cm^2 and a saturated calomel electrode (SCE) as the counter and reference electrodes, respectively. The phase structure of the electrode was analyzed by X-ray diffraction (XRD, Philips. X pert-MPD X) with Cu*Ka* radiation.

2. 2 HRTEM characterization

Microstructure of the RuO_2-ZrO_2 coating was observed using Tecnai G2 F20 S-TWIN (200 KV) field emission TEM in both light field image and electron diffraction pattern of the dark field. The *in situ* phase changes of the composite coating were monitored during an *in situ* annealing process.

2. 3 EXAFS characterization

The K-bound EXAFS of Zr was collected in the 4W1B beam experimental station of Beijing Synchrontron Radiation Laboratory. Energy of the energy storage ring and the maximum beam intensity were 2.2 GeV and 80 mA, respectively. The monochromator was the double crystals of Si(111) face. The K-bound EXAFS of Ru was collected in the BL14W beam experimental station of Shanghai Synchrontron Radiation Laboratory. Energy of the energy storage ring and the maximum beam intensity were determined to be 2.2 GeV and 80 mA, by using the double crystals of Si(111) face as the monochromator. The spectra were recorded under the room temperature transmission mode. The test results of pure cubic ZrO_2 and pure square RuO_2 that had been prepared at 450 ℃ were used as the reference data. The energy calibration was conducted by using the appointed absorption spectral point (17998 eV) of ZrO_2 powder as the baseline. The EXAFS function $k^3x(k)$ was gained after normalization of absorption edge and background reduction. In the equation, energy was converted into the spatial vibration structure from 2 to 15 $Å^{-1}$. Value of $k^3x(k)$ was the weight of k^3. The radial structure function of R space was acquired by Fourier transform and then compared with the radial distribution function of standard oxide samples, getting coordination information of Zr and Ru in samples. On this basis, the corresponding coordination structure was fitted by the ARTEMIS software.

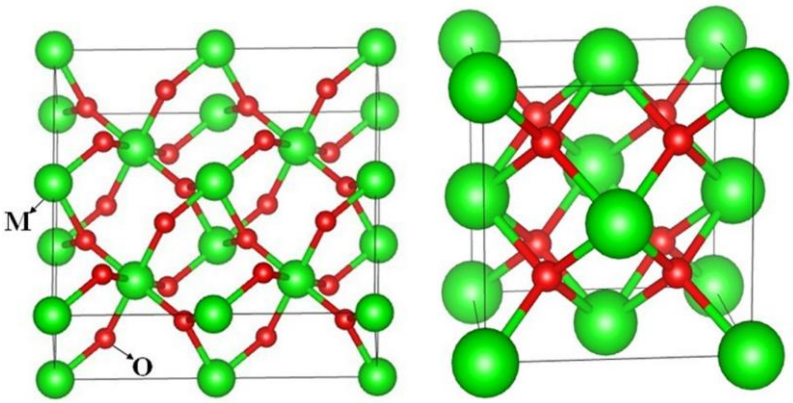

(a) **(b)**

Fig. 1. Super cell of (a) rutile structure of RuO_2 and (b) fluorite structure of ZrO_2

2. 4 Structural calculation

RuO_2 has a rutile structure and its space group is $P4_2/mnm$ (Fig. 1a)[22]. *Ab initio* calculation based on DFT was accomplished by the Vienna *ab initio* simulation package (VASP) software package. Local Density Approximate (LDA) and General Gradient Approximate (GGA) were applied for exchanging correlation potentials. Both were approximation methods. The wave function of system was extended through the plane wave and the cut-off energy of the plane wave was chose to 520 eV. The structure was calculated by self-consistent wave function. The samples were collected from the Brillouin zone using 2 × 2 × 1 super cells and 6 × 6 × 6 Monkhoot-Pack special points, and the convergence standard was the total energy change of each atom lower than 2×10^{-5} eV. To calculate lattice parameters more accurately, structural model of oxide crystal cell was optimized geometrically. The space group of fluorite structure ZrO_2 is $Fm3m$ (Fig. 1b). The 2 × 1 × 1 super cell Zr_8O_{16} was established and four calculation source files (POSCAR, POTCAR, INCAR and KPOINTS) were created under the Linux operating environment. VASP was used for the simulation computation of *ab initio* to the super cells. According to the principle of total energy minimization, the cell volume was optimized and the optimization energy of cells was calculated simultaneously. In computation, the cut-off energy (E_{cut}) was set at 520 eV and the Brillouin zone was determined to be the 4 × 4 × 4 Monkhorst-Pack form in order to assure high calculation accuracy during cell optimization. In the optimization process, ISIF = 3, which means that shape and volume changes of the original cells are allowed. Structural and energy calculation were accomplished in the reciprocal space under the periodic boundary condition.

For RuO_2-ZrO_2, the lattice parameters of rutile and fluorite were calculated under above conditions. To determine cell volume V_0, the total cell energy (E) under 0 K was viewed as the function of volume V. Based on the *ab initio* DFT program, the E-V curve was fitted by the famous Birch-Murnaghan equation (1), getting energy and volume close to equilibrium conditions. Revised and related structure data were acquired:

$$E(V) = E_0 + \frac{B_0}{B_0'}\left[\frac{(V_0/V)^{B_0'}}{B_0'-1}+1\right] - \frac{BV_0}{B_0'-1} \qquad (1)$$

Where E_0 is static energy, V_0 the volume of original cell and B_0' the first-order derivative of pressure intensity of the volume modulus B_0, which is the function of pressure.

3 ELECTRODE STRUCTURE AND ITS RELATION TO CAPACITIVE PERFORMANCE

3. 1 EXAFS analysis

EXAFS of local structure is a very useful tool to analyze the local tissue and fine structure. However, an EXAFS analysis on Ru-Zr has not been reported yet. In this paper, local structural information of the RuO_2-ZrO_2 coating was explored by the EXAFS method to disclose the role of Zr in improvement of conductivity and capacitance of oxide coating with Ru. Fourier transform spatial curves of experimental K^3 and fitted K^3 of Ru-K edge and Z-K edge of RuO_2-ZrO_2 coating prepared by thermal decomposition at 290 ℃ are shown in Fig. 2a. For the convenience of comparison, the curve of RuO_2 sample prepared by thermal decomposition at 450 ℃ is also given.

As can be seen, the central atom Ru and the nearest and second nearest atoms are reflected clearly, which are manifested on the first and second shells in the spectral line. They reflect M-O and M-M bonds, respectively. The first

center shells of the 290 and 450 ℃ samples at 0.18 nm are similar. Both are formed by Ru-O bonds, indicating that they have oxide structures, as RuO_2 belongs to tetragonal system and consists of two 0.18 nm long Ru-O bonds. Peak positions and shapes at two preparation temperatures keep consistent basically, reflecting the high peak intensity. Generally, peak intensities of the second shell differ significantly. RuO_2 coating has perfect Ru-Ru bonding and evident crystalline characteristics, which is proved by the large peak. The peak shape and position are in good accordance with previous researches[23]. The peak of the second shell of the RuO_2-ZrO_2 coating prepared at 290 ℃ is very low, implying the strong instability of Ru-Ru bonding. Particularly, peak positions of two coatings are significantly different, which is caused by their great structural difference. According to preliminary judgment, the dissolving of Zr ions might have generated the displacement of Ru ions.

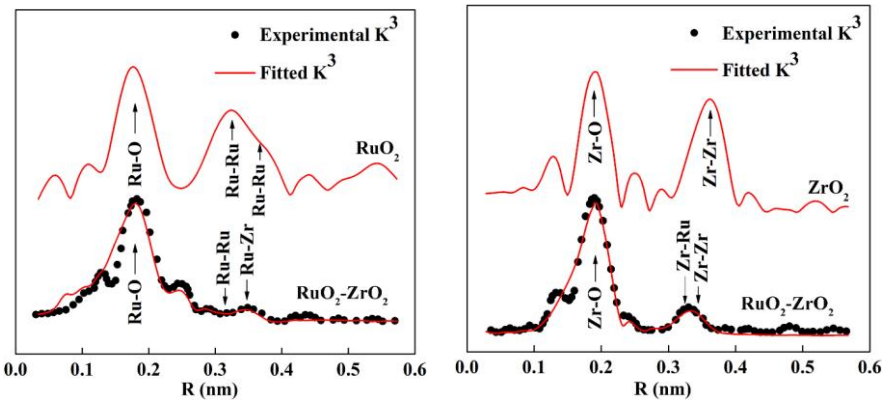

(a) (b)

Fig. 2. Radial distribution function (RDF) curves of RuO_2-ZrO_2: (a) Ru-K edge, and RuO_2 sample prepared at 450 ℃, used as reference; (b) Zr-K edge, and ZrO_2 sample prepared at 450 ℃, used as reference

The Fourier transform spatial curves of experimental K^3 and fitted K^3 of Zr-K edge of the RuO_2-ZrO_2 coating which was prepared by thermal decomposition at 290 ℃ are shown in Fig. 2b. On the curves, the central atom Zr and the nearest and second nearest atoms are reflected clearly, which are manifested on the first and second shells in the spectral line. They reflect M–O and M–M bonds, respectively. For both samples prepared by decomposition at 290 and 450 ℃ respectively, the first shells of Zr all center at 0.2 nm. In other words, peak position at two preparation temperatures keeps constant and the sharp peaks are alike, showing the high peak intensity. The initial fitting of experimental data by combining the ZrO_2 crystal structure reveals that this shell is related to O atoms which are the closest to the central atom. The shell mainly reflects Zr–O bond. This indicates that RuO_2-ZrO_2 coatings prepared at 290 and 450 ℃ are oxides.

The second shell peaks of 290 and 450 ℃ samples are different significantly when the center is at 0.2～0.5 nm. The curve of 290 ℃ sample shows obvious amorphous characteristics. The second shell is Zr-Zr peak and the fitted bond length is 0.362 nm, which is equivalent to the previously reported bond length of low-temperature cubic ZrO_2[24]. This demonstrates that the 450 ℃ sample is a cubic-phase ZrO_2, which is consistent with XRD result (Fig. 3).

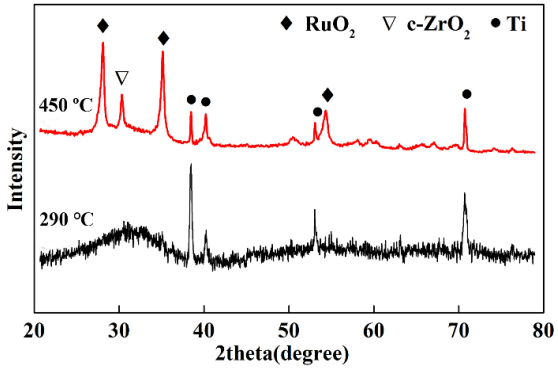

Fig. 3. XRD patterns of Ti/RuO_2-ZrO_2 electrodes prepared at different temperature

The second shell peak of RuO_2-ZrO_2 amorphous coating prepared by thermal decomposition at 290 ℃ is relatively weak, but it still has crystal characteristic spectral line. Therefore, this tissue has an obvious order. It is believed that binary oxide is a disordered amorphous structure, that is, short-range ordering and long-range disordering structure. The second shell has two peaks near 0.31 nm, which are Zr–Ru and Zr–Zr according to fitting. Since Zr–M mixed bonds will be formed by dissolving smaller Ru ions, Zr–Ru and Zr–Zr have far shorter average bond length than the Zr–Zr bond in the 450 ℃ sample (0.362 nm). In a local region, Ru and Zr can be replaced mutually. This fully confirms that the prepared oxide is the amorphous alternative solid solution with short-range ordering and long-range disordering structure. This structure is called the "amorphous solid solution".

The crystallization process of amorphous structure has been analyzed previously by *in situ* electron microscope[25]. Since the prepared material is an unstable amorphous solid solution, a more effective *in situ* analysis is required. The HRTEM images of RuO_2-ZrO_2 coatings are shown in Fig. 4. In Fig. 4a, the RuO_2-ZrO_2 coating presents an amorphous morphology with short-range ordering and long-range disordering structure. Fig. 4b shows that the electron diffraction of this structure is a typical ring pattern, typical for an amorphous structure. However, it can be seen from Fig. 4a and 4d (rectangles) that the whole light field image is dominated by nanoparticles (radius is about 0.29 nm). Buckling and arrangement of distorted lattice points are observed in the enlarged images. Preliminarily, these two types of position ions are viewed in the same region and form the alternative solid solution.

3. 2 *In-situ* analysis of the solid solution structure

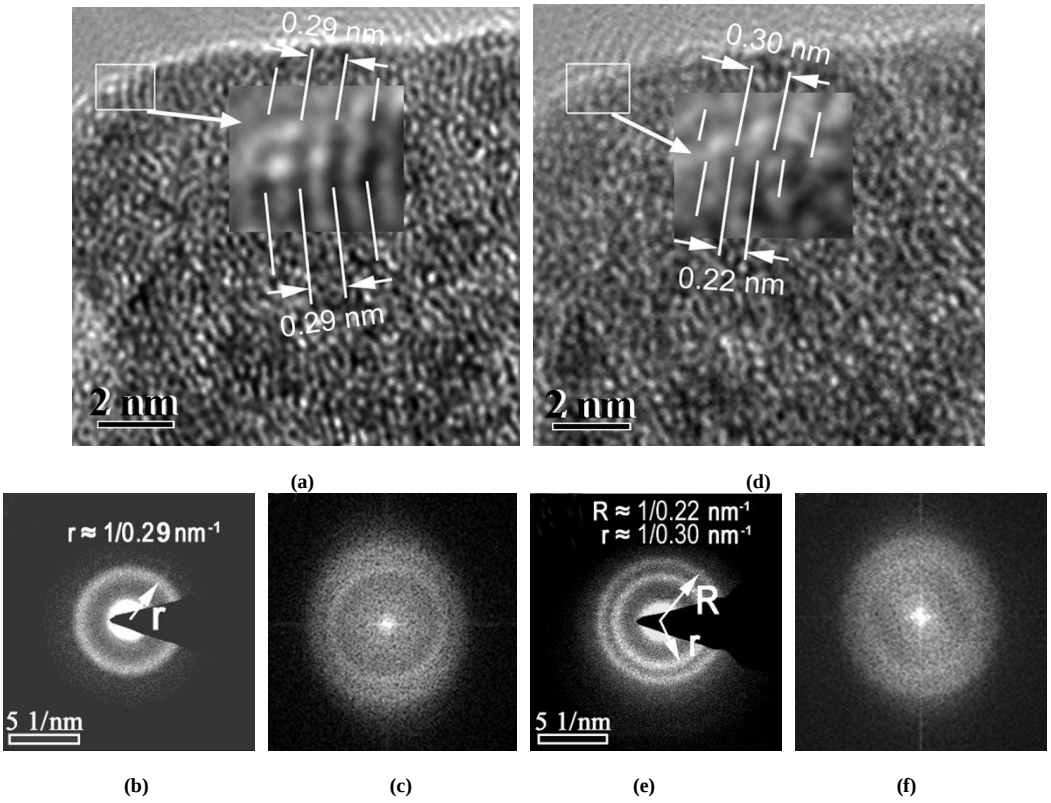

Fig. 4. HRTEM of RuO_2-ZrO_2 coating prepared at 290 ℃: (a) (b) (c) before and (d) (e) (f) after electron beam annealing

HRTEM images taken on *in situ* heating were used to analyze the crystallization temperature of the amorphous solid solution. After 15 min of electron beam annealing, the tissues were still in disordered arrangement, belonging to typical amorphous structure. Re-arrangement of the original lattice points was observed. As seen in the representative region in Fig. 4a, the approximate arrangement of 0.29 nm nanoparticles was changed to the arrangement of 0.30～0.22 nm nanoparticles in Fig. 4d, implying the occurrence of solid decomposition. Fig. 4b, 4c and Fig. 4e, 4f are the SEAD and FFT images of the samples before and after the electron beam annealing, respectively. Compared to Fig. 4b and 4e, Fig. 4c

and 4f show that the original diffusion ring was narrowed slightly and a new ring was developed. From the diffraction ring of SEAD shown in Fig. 4e, the radii of these two regions are calculated to be around 0.30 and 0.22 nm respectively by the above method. This means that one amorphous body and ring have been decomposed into two, respectively. This is consistent with the observation of light field image. According to the *in situ* HRTEM observation during annealing, the original lattice points were rearranged after the annealing of RuO_2-ZrO_2 and one amorphous body was decomposed into two by RuO_2 and ZrO_2. To sum up, this system would produce Ru-Zr oxide with high solid concentration. The phase change belonged to spinodal decomposition reaction[13].

3. 3 Material calculation and confirmation of solid solution structure

According to preliminary judgments based on the above structural characterization, the Ru-Zr oxide prepared by thermal decomposition at a critical crystallization temperature is a kind of amorphous solid solution with short-range ordering and long-range disordering structure. Under equilibrium state, Ru^{4+} would not produce obvious solid solution in ZrO_2[21]. Colomer and Jurado[26] reported that solid solubility of Ru in RuO_2-ZrO_2 solid solution prepared through polymer sol-gel method was 8～10%. Djurado et al[27] found that the solid solubility of RuO_2 in RuO_2-ZrO_2 prepared by thermal decomposition of nitriate oxide was 10～12.5%. Kimura and Goto[28] prepared RuO_2 and Y by MOCVD to stabilize ZrO_2. The XRD result demonstrated that the dissolved load of RuO_2 reached about vol. 25%. However, the RuO_2-ZrO_2 prepared by thermal decomposition in this paper has a high solid solubility. Therefore, it is necessary to calculate its structure to determine the phase structure of microcrystal solid solution and cell parameters.

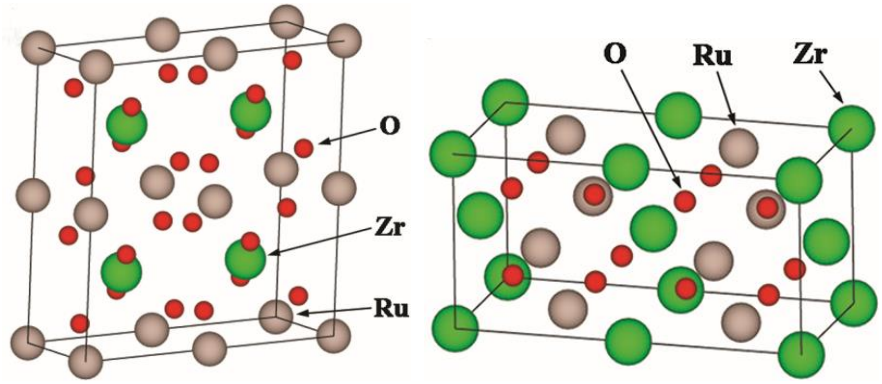

(a) **(b)**

Fig. 5. Structure diagram of the RuO_2-ZrO_2 solid solution based on (a) RuO_2 and (b) ZrO_2

The structure of RuO_2-ZrO_2 is shown in Fig. 5. Different positive ions replace with each other, forming an alternative oxide solid solution. The lattice parameters of RuO_2-ZrO_2 were calculated using rutile and fluorite under above conditions. To determine cell volume V_0, the total cell energy (E) under 0 K was viewed as the function of volume V. Fluorite and rutile are two possible structures of Ru-Zr composite oxide. Their space lattice groups are $Fm3m$ and $P4_2/mnn$, respectively. In fluorite cells, the positive ions are in the center of cube formed by 8 O atoms. In the rutile structure, the positive ions are in the center of deformed octahedron formed by 6 O atoms, including two short O–O bonds and four long O–O bonds[28]. The O–O bond length is an important structural factor that influences hardness of these two structures. The O–O bond length (2.532 Å) of fluorite ZrO_2 under 0 K and 0 GPa and the shortest O–O bond length of rutile ZrO_2 (2.966 Å) (Fig. 6a) were calculated by structural optimization based on *ab initio*. The O–O bond lengths of fluorite and rutile RuO_2 were calculated to be 2.380 and 2.415 Å, respectively (Fig. 6b). Haines[29] also compared them and found that the shortest O–O bond lengths of fluorite and rutile structures were 2.429 and 2.468 Å, which had about 2.0% (fluorite) and 2.2% (rutile) difference as compared to the above results.

The calculated data of cell oxide and fine structural analysis data are listed in Table 1. They were used to investigate the reliability of calculated results. According to the Zr-K edge of fluorite structure calculated by EXAFS method, the Zr–O bond length of the first shell was 2.131 ± 0.004 Å and the coordination number was 4.1, while those of the second shell were 2.208 ± 0.005 and 3.6 Å, respectively. The average bond length was 2.167 Å and the total coordination number was 7.7.

According to the *ab initio* calculation results, the bond length of Zr–O was 2.167 Å and the coordination number was 8. Therefore, the EXAFS method and the *ab initio* were basically equivalent in terms of the average bond length and total coordination number. Nevertheless, they produced significantly different cell parameters of the rutile structure. Firstly, the coordination number of the first shell of Zr–O calculated by EXAFS was 5.2, while that by *ab initio* calculation was 2. Moreover, there was a great gap between two methods with respect to the coordination numbers of the second shell. Based on the above comparison, the RuO_2-ZrO_2 solid solution may be closer to the fluorite structure. Same conclusions could be drawn by comparing structural data of Zr–Ru and Zr–Zr bonds. In other words, structural data of EXAFS and *ab initio* of fluorite structure are closer.

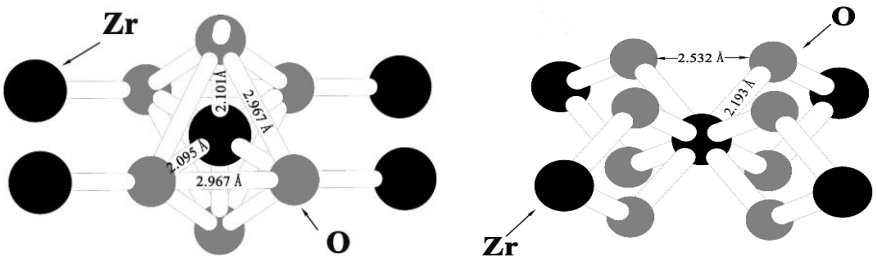

(a) **(b)**

Fig. 6. (a) Rutile and (b) fluorite structures of ZrO_2

3. 4 Discussion on high activity of solid solution structure

The structural analysis confirmed that the prepared RuO_2-ZrO_2 is a type of oxide solid solution with microcrystal arrangement. As a result, the prepared RuO_2-ZrO_2 electrodes have high specific capacitance.

Firstly, different radii and electronic structures of Ru and Zr atoms will cause lattice distortion of solid solution and change the electronic shell structure due to their interaction, thus increasing the active lattice number. These changes will increase electrocatalytic activity of oxides and further bring high "active site density" of oxides. According to Trasatti's opinion[30], active sites of electrode are closely related to electrode structure. Crystal and structural defects are active sites of electrodes. The content of inert ZrO_2 decreases once Ru and Zr form the solid solution. The active lattice number of Ru-containing oxide is doubled and the active site density is increased significantly after mutual solid solution. Electron factors change because of lattice distortion, which can further increase the active site density of oxides.

Table 1. Comparison between the Fitted EXAFS Data of RuO_2-ZrO_2 with *ab initio* Calculation Results

	EXAFS/*ab initio* methods	M–O (Å)	M–M (Å)
Fluorite	Zr–K	4.1×2.131±0.004	5.5×3.486±0.008 (Zr–Ru)
	Edge of EXAFS[a]	3.6×2.208±0.005	1.3×3.667±0.001 (Zr–Zr)
	RuO_2-ZrO_2	{2.167} [b]; <7.7> [c]	{3.521}; <6.8>
	Calculated	8×2.167	8×3.482 (Zr–Ru)
	RuO_2-ZrO_2		4×3.490 (Zr–Zr)
			{3.485}; <12>
Rutile	Ru–K	5.2×2.004±0.006	2.3×3.157±0.008 (Ru–Ru)
	Edge of EXAFS [a]	1.7×2.213±0.005	2.3×3.479±0.002 (Ru–Zr)
	RuO_2-ZrO_2		0.2×3.486±0.001 (Ru–Zr)
		{2.056}; <6.9>	{3.325}; <4.8>
	Calculated	2×1.973	2×3.164 (Ru–Ru)
	RuO_2-ZrO_2	4×1.979	4×3.670 (Ru–Zr)
		{1.977}; <6>	4×3.672 (Ru–Zr)
			{3.570}; <10>

[a] Fitting of Zr–K EXAFS data of RuO_2–ZrO_2 using a rutile template solid-solution structure was also tried, but ended up with poor fitting. This is the same to the fitting of RuO_2–ZrO_2 Ru–K data using a fluorite structure.

[b] Values in {} are the averaged M–O coordination distances.

[c] Values in <> are the total coordination numbers of the same kind.

[d] Values in brackets are from ref.

Secondly, RuO_2-ZrO_2 is a solid solution with microcrystal disordered arrangement and has very high electrochemical roughness R_f. Study on electrochemical roughness of RuO_2-ZrO_2 electrodes showed that the RuO_2-ZrO_2 electrodes prepared at 290 ℃ have the highest electrochemical roughness. This is mainly caused by small diameter of the original microcrystal (about 0.8 nm). Small granularity not only contributes short diffusion distance and easy protolysis in RuO_2-ZrO_2, but can also increase the specific surface area of electrodes and the number of electric active sites[31-33]. Therefore, the smaller the oxide particles are, the higher the active surface will be.

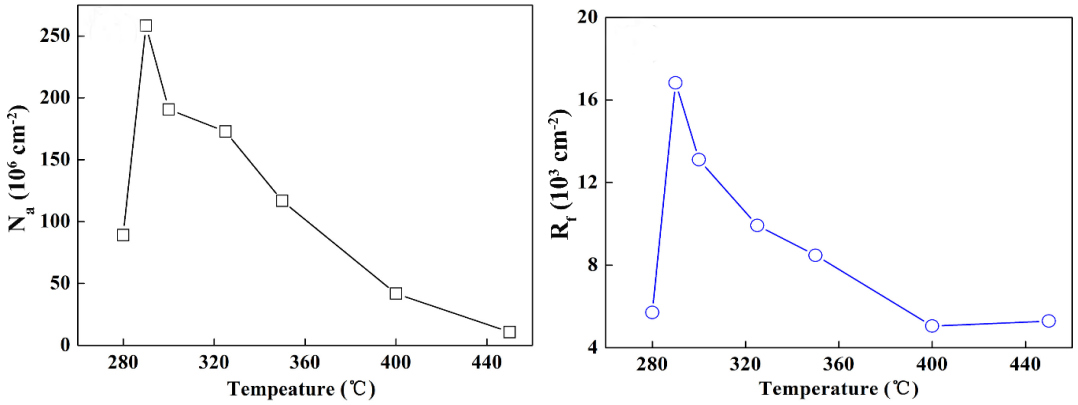

(a) **(b)**

Fig. 7. Effect of preparation temperature on (a) number of active sites and (b) surface roughness of RuO_2-ZrO_2 electrodes

Finally, the microcrystal disordered structure of RuO_2-ZrO_2 is beneficial to increase proton diffusion of coating and the existence of microcrystal leads to high conductivity of electrodes, thus failing to achieve equilibrium between electron and proton conductivity. Therefore, active sites on the coating surface and inside could be fully used.

Calculations of active site and electrochemical roughness are introduced in the reference[34]. The electrochemical active sites and electrochemical roughness data of RuO_2-ZrO_2 electrodes prepared under 280～450 ℃ are given in Fig. 7. The RuO_2-ZrO_2 electrode prepared at 290 ℃ achieves the highest electrochemical active sites and roughness.

Based on above analysis, the RuO_2-ZrO_2 electrode has high electrochemical roughness (R_f) and thereby can get high "active surface". Besides, the interaction of different positive ions in solid solution, or the synergistic catalysis, increases active site density of electrode materials (n_{sites}) significantly. It is the superposition of "active surface" and "synergistic catalysis" that contributes to the unusual high specific capacitance of RuO_2-ZrO_2 electrodes.

To analyze whether the RuO_2-ZrO_2 solid solution involves such superposition, the specific capacitances of several groups of RuO_2-ZrO_2 and RuO_2 prepared under different decomposition temperature are compared in Fig. 8. The action time of the amorphous structure, the second component (element) and the "synergistic catalysis" of interaction of different positive ions could be known.

Firstly, amorphous RuO_2 and nano RuO_2 are compared. Without "synergistic catalysis" of other positive ions and influence of the second component, the specific capacitance is increased by 4.02 times when RuO_2 transits from crystalline structure to the amorphous structure. This indicates that the action time of amorphous structure is generally about 4 times higher than that of crystalline structure.

Secondly, adding the second component increases the specific capacitance by 2.96 times compared to those of crystal RuO_2-ZrO_2 and RuO_2. This indicates that the action time of composition is generally about 3.

If no "synergistic catalysis" occurs, the specific capacitance (Cs) of amorphous RuO_2-ZrO_2 can be calculated according to the following equation (2):

$$C\text{s} = 62.6 \times 4.02 \times 2.96 = 744.9\ \text{F}\cdot\text{g}^{-1} \quad (2)$$

In fact, the specific capacitance of amorphous RuO_2-ZrO_2 solid solution prepared at critical crystallization temperature reached 949 F·g^{-1}. The additional specific capacitance growth of 204.1 F·g^{-1} shall be attributed to "synergistic catalysis" of different positive ions. In other words, the "synergistic catalysis" increases the specific capacitance of RuO_2-ZrO_2 electrodes by 27.5%.

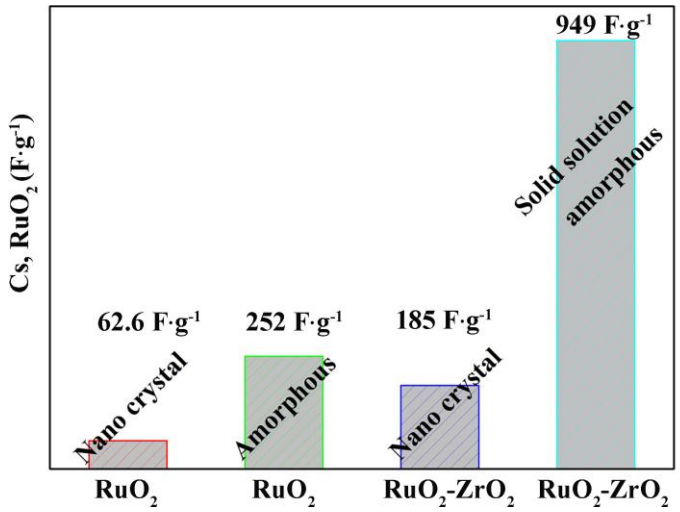

Fig. 8. Comparison of specific capacitances of several electrodes prepared by thermal decomposition method at different temperature. The *Cs* was obtained using galvanostatic charge-discharge test at 5 mA·cm^{-2}

Substantially, adding the second component of the Ru-containing binary oxide is expected to increase the electrocatalytic activity, and specific surface area of RuO_2. It is easy to understand that the synergistic effect between two oxides is needed in order to increase activity of RuO_2. Two oxides should be closely related and form a composite or solid solution for interaction of different positive ions, so "synergistic catalysis" could be used completely. It is difficult to acquire synergistic effect when two oxides are simply mixed. The amorphous structure is divided into topology disorder arrangement and microcrystal disorder arrangement. If the Ru-containing binary oxide belongs to the topology disorder arrangement, the binary oxide is the mixture of two oxides. The second component can be served as a carrier and increase dispersibility and specific capacitance of RuO_2. These are the consequences of increased utilization of RuO_2. This means that the second component will not influence the essential activity of RuO_2 and cause "synergistic effect". The amorphous RuO_2-ZrO_2 solid solution prepared at 290 ℃ makes full use of high activity and high "external active surface" of amorphous material as well as the "synergistic catalysis" of positive ions brought by the solid solution. High specific capacitance of amorphous RuO_2-ZrO_2 solid solution is the results of superposition of multiple advantages. The intrinsic specific capacitance under low circulation speed reaches 1 319.5 F·g^{-1}, which is close to the theoretical specific capacitance of RuO_2.

Further researches on why amorphous structure has higher specific capacitance than existing hydration Ru-containing oxides are needed. Based on previous comparative analyses, short-range ordered microcrystal structure is an important reason because the occurrence of tremendous microcrystal increases the density of high electric conductors significantly. Adding Zr^{4+} expands nanoparticles and is conducive to the diffusion of ions from electric catalytic reaction and reducing resistance of the electric channel, thus increasing the redox ability of materials significantly[35]. However, how to use this active substance with high intrinsic specific capacitance effectively in practical electrode materials is another topic that shall be explored urgently.

4 CONCLUSION

The microstructure of RuO_2-ZrO_2 with high specific capacitance was analyzed by XRD, HRTEM and EXAFS in this paper. It concludes preliminarily that the prepared RuO_2-ZrO_2 is identified as a kind of quasi-amorphous solid solution phase. This solution phase is further explored by *in-situ* annealing based on HRTEM. Combining with *ab initio* calculation, the prepared RuO_2-ZrO_2 is determined to be a type of quasi-amorphous solid solution that has similar structure with fluorite. This quasi-amorphous structure with high solid solubility can explain the high specific capacitance of Ru-Zr oxide. The quasi-amorphous solid solution structure is conducive to "synergistic catalysis" induced by the interaction of positive ions. RuO_2-ZrO_2 coating can gain high "active site density" and "active surface", thus developing high specific capacitance.

REFERENCES

(1) Ferris, A.; Garbarino, S.; Guay, D.; Pech, D. 3*D* RuO_2 microsupercapacitors with remarkable areal energy. *Adv. Mater.* **2015**, 27, 6625–6629.

(2) Wang, Y. L.; Gu, D. W.; Guo, J. R.; Xu, M. Y.; Sun, H. S.; Li, J. S.; Wang, L.; Shen, L. J. Maximized energy density of RuO_2//RuO_2 supercapacitors through potential dependence of specific capacitance. *Chemelectrochem* **2020**, 7, 928–936.

(3) Park, S.; Shin, D.; Yeo, T.; Seo, B.; Hwang, H.; Lee, J.; Choi, W. Combustion-driven synthesis route for tunable TiO_2/RuO_2 hybrid composites as high-performance electrode materials for supercapacitors. *Chem. Eng. J.* **2020**, 384, 123269–5.

(4) Jow, J. J.; Lai, H. H.; Chen, H. R.; Wang, C. C.; Wu, M. S.; Ling, T. R. Effect of hydrothermal treatment on the performance of RuO_2-Ta_2O_5/Ti electrodes for use in supercapacitors. *Electrochim. Acta* **2010**, 55, 2793–2798.

(5) Hu, C. C.; Wang, C. W.; Wu, T. H.; Chang, K. H. Anodic composite deposition of hydrous RuO_2-TiO_2 nanocomposites for electrochemical capacitorss. *Electrochim. Acta* **2012**, 85, 590–598.

(6) Xiang, D.; Yin, L. W.; Wang, C. X.; Zhang, L. Y. High electrochemical performance of RuO_2-Fe_2O_3 nanoparticles embedded ordered mesoporous carbon as a supercapacitor electrode material. *Energy* **2016**, 106, 103–111.

(7) Gránásy, L.; James, P. F. Non-classical theory of crystal nucleation: application to oxide glasses: review. *J. Non–Cryst. Solids* **1999**, 253, 210–230.

(8) Wong, W. Y.; Ho, C. L. Heavy metal organometallic electrophosphors derived from multi-component chromophores. *Coord. Chem. Rev.* **2009**, 253, 1709–1758.

(9) Simon, P.; Gogotsi, Y. Materials for electrochemical capacitors. *Nat. Mater.* **2008**, 7, 845–854.

(10) Wang, G.; Zhang, L; Zhang, J. A review of electrode materials for electrochemical supercapacitors. *Chem. Soc. Rev.* **2012**, 41, 797–828.

(11) Gonzâez, A.; Goikolea, E.; Barrena, J. A.; Mysyk, R. Review on supercapacitors: technologies and materials. *Sust. Energ. Rev.* **2016**, 58, 1189–1206.

(12) Shi, F.; Li, L.; Wang, X.; Gu, C.; Tu, J. Metal oxide/hydroxide-based materials for supercapacitors. *RSC Adv.* **2014**, 4, 41910–41921.

(13) Zhu, J. Q.; Wang, X.; Yi, Z.; Tang, Z.; Wu, B.; Tang, D.; Lin, W. Stability of solid-solution phase and the nature of phase separation in Ru-Zr-O ternary oxide. *J. Phys. Chem. C* **2012**, 116, 25832–25839.

(14) Ma, J. D.; Zuo, J.; Jiang, C. H.; Khan, D. F.; Zhang, H. A.; Zhu, J. Q. Effects of temperature on the capacitive performance of Ti/40%RuO_2-60%ZrO_2 electrodes prepared by thermal decomposition method. *J. Electroanal. Chem.* **2017**, 789, 133–139.

(15) Siegrist, T.; Jost, P.; Volker, H.; Woda, M.; Merkelbach, P.; Schlockermann, C.; Wuttig, M. Disorder-induced localization in crystalline phase-change materials. *Nat. Mater.* **2011**, 10, 202–208.

(16) Blakemore, J. D.; Mara, M. W.; Kushner-Lenhoff, M. N.; Schley, N. D.; Konezny, S. J.; Rivalta, I.; Negre, C. F. A.; Snoeberger, R. C.; Kokhan, O.; Huang, J.; Stickrath, A.; Tran, L. A.; Parr, M. L.; Chen, L. X.; Tiede, D. M.; Batista, V. S.; Crabtree, R. H.; Brudvig, G. W. Characterization of an amorphous iridium water-oxidation catalyst electrodeposited from organometallic precursors. *Inorg. Chem.* **2013**, 52, 1860–1871.

(17) Tsuji, E.; Imanishi, A.; Fukui, K.; Nakato, Y. Electrocatalytic activity of amorphous RuO_2 electrode for oxygen evolution in an aqueous solution. *Electrochim. Acta* **2011**, 56, 2009–2016.

(18) Patake, V. D.; Pawar, S. M.; Shinde, V. R.; Gujar, T. P.; Lokhande, C. D. The growth mechanism and supercapacitor study of anodically deposited amorphous ruthenium oxide films. *Curr. Appl. Phys.* **2010**, 10, 99–103.

(19) Ishimaru, M.; Hirata, A.; Naito M. Electron diffraction study on chemical short-range order in covalent amorphous solids. *Meth. Phy. Res. Sect. B* **2012**, 277, 70–76.

(20) Playford, H.; Keen, D.; Tucker, M. Local structure of crystalline and amorphous materials using reverse monte carlo methods. *Neutron News* **2016**, 27, 17–21.

(21) Hrovat, M.; Holc, J.; Kolar, D. Thick film ruthenium oxide/yttria-stabilized zirconia-based cathode material for solid oxide fuel cells. *Solid State Ionics* **1994**, 68, 99–103.

(22) Altwasser, S.; Glaser, R.; Lo, A.; Liu, P.; Chao, K.; Weitkamp, J. Incorporation of RuO_2 nanoparticles into MFI-type zeolites. *Micropor. Mesopor. Mat.* **2006**, 89, 109–122.

(23) Chang, C. J.; Chu, Y. C.; Yan, H. Y.; Liao, Y. F.; Chen, H. M. Revealing the structural transformation of rutile RuO_2 via *in situ* X-ray absorption spectroscopy during the oxygen evolution reaction. *Dalton T.* **2019**, 48, 7122–7129.

(24) Nagai, Y.; Yamamoto, T.; Tanaka, T.; Yoshida, S.; Nonaka, T.; Okamoto, T.; Suda, A.; Sugiura, M. X-ray absorption fine structure analysis of local structure of CeO_2-ZrO_2 mixed oxides with the same composition ratio (Ce/Zr = 1). *Catal. Today* **2002**, 74, 225–234.

(25) Biskupek, J.; Kaiser, U.; Falk, F. Heat and electron-beam-induced transport of gold particles into silicon oxide and silicon studied by *in situ* high-resolution transmission electron microscopy. *Microsc.* **2008**, 57, 83–89.

(26) Colomer, M. T.; Jurado, J. R. Preparation and characterization of gels of the ZrO_2-Y_2O_3-RuO_2 system. *J. Non-Cryst. Solids* **1997**, 217, 48–54.

(27) Djurado, E.; Roux, C.; Hammou, A. Synthesis and structural characterization of a new system: ZrO_2-Y_2O_3-RuO_2. *J. Eur. Ceram. Soc.* **1996**, 16, 767–771.

(28) Kimura, T.; Goto, T. Preparation of RuO_2-YSZ nano-composite films by MOCVD. *Surf. Coat. Tech.* **2003**, 167, 240–244.

(29) Haines, J.; Ger, J. M.; Schulte O. Pa3 modified fluorite-type structures in metal dioxides at high pressure. *Science* **1996**, 271, 629–631.

(30) Trasatti, S. Electrocatalysis: understanding the success of DSA®. *Electrochim. Acta* **2000**, 45, 2377–2385.

(31) Sugimoto, W.; Yokoshima, K.; Murakami, Y.; Takasu, Y. Charge storage mechanism of nanostructured anhydrous and hydrous ruthenium-based oxides. *Electrochim. Acta* **2006**, 52, 1742–1748.

(32) Pico, F.; Morales, E.; Fernandez, J. A.; Centeno, T. A.; Ibañez, J.; Rojas, R. M.; Amarilla, J. M.; Rojo, J. M. Ruthenium oxide/carbon composites with microporous or mesoporous carbon as support and prepared by two procedures. a comparative study as supercapacitor electrodes. *Electrochim. Acta* **2009**, 54, 2239–2245.

(33) Kim, H.; Popov, B. N. Characterization of hydrous ruthenium oxide/carbon nanocomposite supercapacitors prepared by a colloidal method. *J. Power Sources* **2002**, 104, 52–61.

(34) Nanni, L.; Polizzi, S.; Benedetti, A.; De Battisti, A. Morphology, microstructure, and electrocatalytic properties of RuO_2-SnO_2 thin films. *J. Electrochem. Soc.* **1999**, 146, 220–225.

(35) Chabanier, C.; Irissou, E.; Guay, D.; Pelletier, J.; Sutton, M.; Lurio, L. Hydrogen absorption in thermally prepared RuO_2 electrode. *Electrochem. Solid-State Lett.* **2002**, 5, E40–E42.